

Observations of a $z = 1.44$ Dusty, Ultraluminous Galaxy and Implications for Deep Sub-mm Surveys

Arjun Dey^{1,2}

Department of Physics & Astronomy, The Johns Hopkins University, Baltimore, MD 21218
dey@noao.edu

James R. Graham

Astronomy Department, University of California at Berkeley, CA 94720
jrg@astro.berkeley.edu

Rob J. Ivison³

Institute for Astronomy, Dept. of Physics & Astronomy, University of Edinburgh, Blackford Hill,
Edinburgh EH9 3HJ, Scotland, UK
rji@roe.ac.uk

Ian Smail⁴

Dept. of Physics, University of Durham, South Road, Durham DH1 3LE, England, UK
ian.smail@durham.ac.uk

Gillian S. Wright

Institute for Astronomy, Dept. of Physics & Astronomy, University of Edinburgh, Blackford Hill,
Edinburgh EH9 3HJ, Scotland, UK
G.Wright@roe.ac.uk

and

Michael C. Liu

Astronomy Department, University of California at Berkeley, CA 94720
mliu@astro.berkeley.edu

Accepted for publication in the Astrophysical Journal

¹Hubble Fellow

²Present address: NOAO, 950 N. Cherry Ave., Tucson, AZ 85719

³PPARC Advanced Fellow

⁴Royal Society University Research Fellow

ABSTRACT

We present new near-infrared and optical spectroscopic observations which confirm the redshift of the $z = 1.44$ extremely red object ERO J164502+4626.4 (object # 10 of Hu & Ridgway 1994; formerly known as ‘HR 10’ or ‘[HR94] 10’) and a *Hubble Space Telescope* image which reveals a reflected-S-shaped morphology at (rest-frame) near-ultraviolet wavelengths. The contrast between the rest-frame far-red ($\lambda\lambda 8200 - 9800\text{\AA}$) and near-UV ($\lambda\lambda 2900 - 3900\text{\AA}$) morphologies suggests that the central regions of the galaxy are heavily obscured by dust and that the galaxy is most likely an interacting or disturbed system. We also present new photometry of this object at $450\mu\text{m}$, $850\mu\text{m}$ and $1350\mu\text{m}$ obtained using the SCUBA submillimeter camera on the James Clerk Maxwell Telescope. Our sub-mm data are extremely sensitive to emission from cold dust at high redshift. The rest-frame spectral energy distribution of ERO J164502+4626.4 is best understood in terms of a highly reddened stellar population with ongoing star formation, as originally suggested by Graham & Dey (1996). The new submillimeter data presented here indicate that the remarkable similarity to ultraluminous infrared galaxies (ULIRGs) such as Arp 220 and Mrk 231 extends into the rest-frame far-infrared which bears the signature of thermal emission from dust, presumably heated by young stars. ERO J164502+4626.4 is extremely luminous ($L \approx 7 \times 10^{12} h_{50}^{-2} L_{\odot}$) and dusty ($M_{\text{dust}} \approx 7 \times 10^8 (T_{\text{dust}}/40\text{K})^{-5} h_{50}^{-2} M_{\odot}$). If its luminosity is powered by young hot stars, then ERO J164502+4626.4 is forming stars at the prodigious rate of $\dot{M} = 1000 - 2000 h_{50}^{-2} M_{\odot} \text{yr}^{-1}$. We conclude that ERO J164502+4626.4 is a distant analogue of the nearby ULIRG population, the more distant or less luminous counterparts of which may be missed by even the deepest existing optical surveys. The sub-mm emitters recently discovered by deep SCUBA surveys may be galaxies similar to ERO J164502+4626.4 (but perhaps more distant). This population of extremely dusty galaxies may also contribute significantly to the cosmic sub-mm background emission.

Subject headings: cosmology: observations — cosmology: early universe — galaxies: evolution — galaxies: formation — galaxies: starburst — galaxies: individual: ERO J164502+4646.4 (HR 10 or [HR94] 10)

1. Introduction

Near-infrared (near-IR) imaging surveys have resulted in the discovery of a population of infrared-bright, extremely red objects (‘EROs’), which may be of significance to studies of galaxy evolution. EROs, which we define in this paper as having observed optical-near-IR colors $R-K > 6$, have been identified both in the field, and around high-redshift radio galaxies and quasars (Elston, Rieke, & Rieke 1988, 1989, 1991; McCarthy, Persson, & West 1992; Eisenhardt & Dickinson 1992; Graham et al. 1994; Hu & Ridgway 1994; Dey, Spinrad, & Dickinson 1995). Images of EROs from ground-based telescopes show that they are spatially extended on scales of $\sim 0''.5$. This suggests that EROs are probably galaxies rather than stellar objects (e.g., brown dwarfs). Most EROs were not *a priori* selected as radio sources and are generally radio quiet. Extremely faint optically ($R > 24.5$), their distances and spectral properties (i.e., whether they are normal or active galaxies) remain unknown.

The extreme colors of these objects might be attributed either to an old stellar population, or to a younger stellar population reddened by dust (Graham & Dey 1996, hereafter GD96; Yamada et al. 1997). The spectral energy distributions (hereafter SEDs) of the reddest EROs known are inconsistent with unreddened old populations at any redshift, and suggest that they must be highly reddened starburst galaxies, perhaps the distant counterparts of the local ultraluminous infrared galaxies (ULIRGs; e.g., Soifer et al. 1984) discovered by the *Infrared Astronomical Satellite (IRAS)*.

Most EROs have been discovered serendipitously, and their space densities are therefore uncertain. Some measurements suggest that the most extreme EROs (i.e., those as red as ERO J164502+4626.4) are as abundant as quasars, with a surface density in blank fields $\approx 0.01 \text{ arcmin}^{-2}$ (Hu & Ridgway 1994; Cowie et al. 1994). More recent measurements suggest that the surface density of objects with $R - K' \geq 6$ and $K' \leq 17.5$ is $\approx 0.1 \text{ arcmin}^{-2}$ (Beckwith et al. 1998) with fainter EROs possibly having even higher surface densities ($\approx 0.7 \text{ arcmin}^{-2}$ for EROs with $K' \leq 20$; Eisenhardt et al. 1998). There is also some evidence that their surface density is higher in regions around high-redshift radio galaxies and quasars compared with the general field (e.g., Aragon-Salamanca et al. 1994; Dey, Spinrad, & Dickinson 1995; Yamada et al. 1997). An obvious interpretation of this result is that the EROs are clustered around and hence physically associated with the distant, luminous AGN, which would imply that EROs are at $z \sim 1 - 3$ and their rest-frame optical luminosities are 5–20 times more luminous than unevolved L^* ellipticals at the same redshifts. Alternatively, this excess number density may suggest that our samples of distant luminous AGN are biased due to gravitational lensing by foreground mass concentrations with which the EROs are associated.

Given that the EROs may constitute a significant population in our Universe, it is important to understand their nature. In this paper we present new optical, near-IR and sub-mm observations (§ 2) of ERO J164502+4626.4, an ERO discovered in the field of the $z = 3.8$ quasar PC1643+4631

(object # 10 of Hu & Ridgway 1994)⁵. Our new observations convincingly demonstrate that ERO J164502+4626.4 is a $z = 1.44$ luminous, dusty starburst galaxy, a distant counterpart of local ULIRGs like Arp 220 and Mrk 231, as originally suggested by GD96 (§ 3). The detection of ERO J164502+4626.4 at sub-mm wavelengths, and the relatively large surface density of the ERO population suggests that these objects may be candidates for the sub-mm emitters recently discovered in deep SCUBA surveys (Smail et al. 1997, Blain et al. 1999a, Hughes et al. 1998, Barger et al. 1998), and we briefly discuss this possibility and its consequences in § 3.5.

We assume $H_0 = 50h_{50} \text{ km s}^{-1} \text{ Mpc}^{-1}$, $q_0 = 0.5$, and $\Lambda = 0$ throughout. For this cosmology, the luminosity distance of ERO J164502+4626.4 is $10.53h_{50}^{-1} \text{ Gpc}$. For $q_0=0.1$, the luminosity distance is larger by a factor of 1.286.

2. Observations and Results

2.1. HST WFPC2 Imaging

The field of PC 1643+4631 was observed using the Wide Field Planetary Camera 2 (WFPC2; Trauger et al. 1994, Holtzman et al. 1995) on the refurbished *Hubble Space Telescope (HST)* through the F814W filter on UT 1997 May 7. A position angle (P.A.) of 68.2° was used in order to simultaneously observe both ERO J164502+4626.4 and ERO J164457+4626.0 (objects # 10 and 14 of Hu & Ridgway 1994). Both objects were targetted on the WF CCDs in order to optimize the detection of faint diffuse emission. We obtained 4 exposures over 2 orbits with the telescope dithered by $\approx 0''.7$ between orbits. The total integration time was 5300 sec. The images resulting from the calibration pipeline were corrected for cosmic rays, registered and coadded. Flux calibration was performed using the photometric zero points of Holtzman et al. (1995). The final image reaches a 3σ limiting surface brightness of $26.77 \text{ AB mag arcsec}^{-2}$ in an $1\Box''$ aperture.

The WFPC2 F814W image of ERO J164502+4626.4 (rotated to a normal orientation where north is up and east is to the left) is shown in figure 1. The galaxy is extended by roughly $0''.9$ in P.A. $\approx -21^\circ$ in a reflected ‘S-shaped’ morphology that is suggestive of an interacting system or spiral / tidal arms. We spatially coregistered the *HST* image with the near-IR *K*-band image of GD96 using 16 common objects; the relative positional accuracy is better than $0''.02$. A comparison of the F814W and *K*-band images reveals that the bulk of the near-IR emission arises from a region of low optical flux, in between the two bright lobes of optical emission (the ends of the reflected ‘S’; figure 2). The brightest region of optical emission is *not* cospatial with the peak of the near-IR emission, but instead lies $\approx 0''.4$ south of it (figure 2).

In a $3''$ diameter aperture, ERO J164502+4626.4 is found to have a magnitude of $24.6 \pm 0.1 \text{ AB}$

⁵This ERO has been previously referred to as ‘HR 10’ and ‘[HR94] 10’ (e.g., Graham & Dey 1996; Cimatti et al. 1998). The nomenclature used in this paper follows the IAU recommendations for source names.

mag (at $\lambda_{\text{obs}} \approx 7930\text{\AA}$) or, equivalently, a Cousins I -band magnitude of $I_C \approx 24.2$. The color of ERO J164502+4626.4 in this aperture is then $I_C - K \approx 5.8 \pm 0.1$, consistent with the values quoted by GD96 and HR94. The magnitudes of the northern and southern optical lobes, measured in apertures of diameter $0''.5$, are 26.4 ± 0.1 AB mag and 26.0 ± 0.1 AB mag respectively.

2.2. Optical Spectroscopy

We obtained optical spectra of ERO J164502+4626.4 on U.T. 1998 May 4 using the Low Resolution Imaging Spectrometer (LRIS; Oke et al. 1995) at the Cassegrain focus of the Keck II Telescope. The observations were made in good seeing (FWHM $\approx 0''.6 - 0''.8$) through a $1''.0$ wide slit oriented in P.A. = 66.2° . LRIS was configured with the 400 line mm^{-1} grating ($\lambda_{\text{blaze}} \approx 8500\text{\AA}$; $\Delta\lambda_{\text{FWHM}} \approx 10\text{\AA}$), and the spectra cover the wavelength range $\lambda\lambda 5910 - 9730\text{\AA}$. The total exposure time was 3 hours, and the target was dithered along the slit after every 30 min sub-exposure in order to allow for proper fringe removal and sky subtraction. Wavelength calibration was performed using NeAr lamps obtained immediately following the ERO J164502+4626.4 observations, and relative flux calibration was performed using observations of the standard stars Wolf 1346 and Feige 34 (Massey et al. 1988, Massey & Gronwall 1990). Although the observations were made under non-photometric conditions, the spectrum was scaled to an absolute scale using published photometry (GD96, Hu & Ridgway 1996).

The sky-subtracted two-dimensional spectrum is shown in figure 3, and the extracted one-dimensional spectrum (extracted in a $1''.7$ aperture) and the corresponding 1σ errors are presented in figure 4. The notable features in the optical spectrum are a strong emission line at $\lambda 9090\text{\AA}$ (which corresponds to the [OII] $\lambda\lambda 3726, 3729$ doublet at $z = 1.439$) and a very red continuum emission ($F_\nu \propto \nu^{-5.5 \pm 0.5}$ in the wavelength range $\lambda\lambda 6500 - 9000\text{\AA}$). The signal-to-noise ratio in the continuum is too poor to convincingly detect any absorption lines or spectral breaks. The measured flux, FWHM and rest frame equivalent width of [OII] $\lambda\lambda 3726, 3729$ are presented in Table 1.

2.3. Near-Infrared Spectroscopy

Near-IR spectroscopy of ERO J164502+4626.4 was obtained using the Cryogenic Spectrograph (CRSP; Joyce 1995) at the Cassegrain focus of the KPNO 4m Mayall Telescope on the night of U.T. 1997 June 21. CRSP was configured with grating # 4 (200 line mm^{-1} , $\lambda_{\text{blaze}} = 3.0\ \mu\text{m}$, dispersion $\approx 12\text{\AA pixel}^{-1}$) used in 2nd order and a $1''.0$ slit to provide a resolution FWHM of $0.0042\ \mu\text{m}$ over the wavelength range $1.444\ \mu\text{m}$ to $1.750\ \mu\text{m}$. Observations of ERO J164502+4626.4 were obtained by dithering the object along the slit; each dither sequence consisted of five equally spaced target positions along the slit separated by $8''$. The slit was oriented at P.A.= 59.3° in order to include a nearby galaxy (object 6 in figure 1; our notation follows that of HR94) to aid in accurately coadding the data. Each individual observation was 3 min long, and the total exposure time was

195 min. The seeing during the observations was typically $0''.8$ in the K -band. The atmospheric absorption was corrected using observations of the telluric standard HR6064 (G1V) obtained at various airmasses both preceding and following the ERO J164502+4626.4 observations.

The spectral frames were dark-subtracted, flat-fielded, rectified, sky-subtracted, and coadded by using object 6 (see figure 1) to determine the accurate relative offsets. The sky subtraction of each spectral frame was performed using a ‘local’ sky constructed from the median of the four preceding and four following frames. The summed two-dimensional spectrum is shown in the upper panel of figure 3. The extracted spectrum was divided by the mean spectrum of the telluric standards to correct for the telluric absorption, and corrected for the stellar features by multiplying by the mean spectrum of a G0V star constructed by averaging the spectra of HD109358 and HR5868 from the near-IR spectral atlas of Lancon and Rocca-Volmerange (1992). Since the continuum emission from ERO J164502+4626.4 is only marginally detected in these observations, the telluric corrections are largely unnecessary, but also provide us with a rough relative flux calibration. The resulting spectrum was then scaled by a constant to be consistent with the H -band flux of ERO J164502+4626.4.

The calibrated near-IR spectrum of ERO J164502+4626.4 is shown in figure 5, and clearly shows the emission line detected by GD96. The line is narrow, and appears to be resolved into at least two components. The ratio of the wavelengths of the two brighter components roughly matches the ratio of $[\text{N II}]\lambda 6584 / \text{H}\alpha$, and is consistent with the original identification (by GD96) of the line as $\text{H}\alpha + [\text{N II}]$. The extracted spectrum also shows a weak feature at the expected location of the $[\text{SII}]\lambda\lambda 6717, 6731$ doublet. However, given the signal-to-noise ratio of the present data, we caution that the $[\text{NII}]\lambda 6584$ and the $[\text{SII}]\lambda\lambda 6717, 6731$ detections are marginal, and should be treated accordingly (e.g., figure 5).

The emission line measurements are presented in Table 1. The numbers in this table were derived by using the SPECFIT software (Kriss 1994) as implemented in *IRAF* to fit Gaussians to the emission lines in the calibrated unsmoothed spectrum. The $\text{H}\alpha$ and $[\text{NII}]\lambda 6584$ emission lines were fit jointly by requiring the two features to have equal width and holding the ratio of their central wavelengths constant. The new high-resolution near-IR observation presented here provides a more accurate measurement of the equivalent widths and FWHMs of the $\text{H}\alpha$ and $[\text{NII}]$ emission lines. In these new higher spectral resolution data, the emission lines are found to be narrower and have smaller equivalent widths than those derived by GD96.

2.4. Sub-mm Photometry

Data were obtained during 1997 June, July and December, and 1998 January and February using the Sub-mm Common-User Bolometer Array (SCUBA; Holland et al. 1998). SCUBA has two arrays of bolometric detectors which are operated at 0.1 K to achieve sky background-limited performance on the telescope at 350–450 and 750–850 μm . Three extra bolometers — ‘photometric

pixels’ optimized for use at 1100, 1350 and 2000 μm — are positioned around the long-wave array.

Photometry of sources significantly smaller than the beam are generally performed using the central pixels of each array, which are aligned to within an arcsecond of each other, or the photometric pixels. The best photometric accuracy is achieved by averaging the source signal over a slightly larger area than the beam, so the secondary mirror was ‘jiggled’ in a filled-square, 9-point pattern, covering $4'' \times 4''$. During the ‘jiggle’ the secondary mirror was chopped azimuthally by $60''$ at 6.944 Hz. After the first 9 sec ‘jiggle’, the telescope was nodded azimuthally to the reference position (subsequently every 18 sec). At 450 μm and 850 μm , we spent 260 min on source, with a further 165 min at 1350 μm .

Skydips were performed before, during and after the target measurements to determine the zenith opacities, and the telescope pointing accuracy was checked regularly using 1633+382 and 3C 345. All data were calibrated against observations of Mars and Uranus. The observing conditions during the SCUBA runs were excellent, especially during the early 1998 observing periods.

Reduction of the 450 μm and 850 μm data consisted of taking the measurements from the central bolometer, rejecting spikes, and averaging over 18 sec time intervals. The signal detected by all the bolometers is dominated by spatially correlated sky emission (Ivison et al. 1998a), so data from the adjacent rings of bolometers were treated in a similar manner. The residual sky background was removed using the median of the inner two rings of pixels, after rejecting those with excessive noise. This reduced the noise-equivalent flux density at 850 μm to around 90 mJy Hz $^{-1/2}$, suggesting that the effects of rapid sky variability have been removed entirely. Reduction of the 1350 μm data followed a similar process, though without the removal of sky noise.

At 850 μm , we find a clear detection of ERO J164502+4626.4 at a level well above the expected extrapolation of the weak radio emission; at 450 and 1350 μm , the detection significance is lower, but the measured flux densities are $> 3\sigma$ detections, and are entirely consistent with thermal emission from optically thin dust. The flux density measurements at 450 μm , 850 μm and 1350 μm are reported in Table 2.

The 850 μm and 1350 μm flux densities reported in this paper are roughly half the values reported by Cimatti et al. (1998). Our more extensive dataset was obtained during exceptional observing conditions, as evident from the 450 μm detection, and we can exclude a substantially higher flux with some confidence. Furthermore, our data were obtained using a single telescope with internally consistent flux calibration, and the 450 μm and 850 μm photometric data were obtained simultaneously. Hence, the relative photometry (and the derived spectral index) are self consistent and more accurate than other sub-mm measurements of ERO J164502+4626.4 presented to date. There also exist 95 μm and 175 μm observations of ERO J164502+4626.4 obtained with the *Infrared Space Observatory (ISO)*, which can provide additional consistency checks on the sub-mm observations. We will report on these *ISO* observations in a forthcoming work by Ivison et al. (1999).

3. Discussion

3.1. Spectral Properties

The spectroscopic observations presented in this paper confirm the $z = 1.440$ redshift of the galaxy by resolving the emission line reported by GD96 into two components which match the H-alpha + [NII] identification, the detection of the [OII] $\lambda\lambda 3726, 3729$ doublet, and the marginal detection of the [SII] $\lambda\lambda 6717, 6731$ emission lines at the same redshift.

The $H\alpha/[NII]\lambda 6584$ ratio ($\gtrsim 2.4$) and the relatively narrow linewidths of the [OII] and $H\alpha$ emission lines suggest that the ionization is more likely to be due to young, hot stars than an active galactic nucleus (AGN). The spectrum of ERO J164502+4626.4 is similar to that observed in local star-forming galaxies (e.g., Kennicutt 1992). The FWHM (deconvolved FWHM $\approx 260 \text{ km s}^{-1}$) of the [OII] doublet and equivalent width of the $H\alpha$ emission line from ERO J164502+4626.4 are more typical of star-forming galaxies than AGN (e.g., Liu & Kennicutt 1995). However, since an AGN could be hidden behind dust and rendered invisible at rest frame optical and ultraviolet wavelengths, a firm statement on the nature of the energy source must await future mid- and far-infrared spectroscopy. In the following discussion, we assume that young stars power the entire far-infrared emission from ERO J164502+4626.4.

3.2. Morphology

The *HST* WFPC2 image (figures 1 and 2) clearly shows that ERO J164502+4626.4 has an elongated and distorted morphology. At a redshift of 1.44, the WFPC2 F814W filter samples the rest-frame wavelength range $\lambda\lambda 2900\text{--}3900$ (i.e., roughly rest-frame *U*-band light), which includes the [O II] $\lambda\lambda 3726, 3729$ emission doublet. The equivalent width of this emission feature in ERO J164502+4626.4 implies that the emission line contamination in the F814W filter is $\lesssim 8\%$; the observed morphology is therefore dominated by the continuum emission from the galaxy. Since the filter samples the continuum at near-UV wavelengths just shortward of the 4000\AA break, the morphology observed in the *HST* image only reflects the distribution of UV bright populations (i.e., hot, young stars), and in addition may be heavily modified by the distribution of dust in the galaxy. The peculiar UV morphology may be due to spiral arms, tidal features or something more complex, and suggests that ERO J164502+4626.4 may be an interacting or distorted system.

The most striking aspect of the rest frame near-UV morphology is that it is very different from the rest frame far-red morphology observed in the *K*-band: the red emission is more symmetric (at least at the $0''.6$ resolution of the GD96 ground-based image) and peaks in a region where the near-UV emission falls to a minimum, approximately at the center of the reflected S-shaped structure seen in the WFPC2 image (figure 2). Since the far-red emission in galaxies is generally dominated by late type giant stars and an older main sequence population and the near-UV emission is dominated by younger, hotter stars, the observed morphological difference could be partly due to

spatially distinct populations, with the older stars being more centrally concentrated (perhaps in a bulge?) compared to the younger stars (perhaps in a disk or tidal arms?).

Is it possible that the UV morphology is dominated by young super star clusters? The specific luminosities of the northern and southern lobes observed in the near-UV ($\lambda_{rest} \approx 3250\text{\AA}$) image are $5.4 \times 10^{27} h_{50}^{-2} \text{ erg s}^{-1} \text{ Hz}^{-1}$ and $7.9 \times 10^{27} h_{50}^{-2} \text{ erg s}^{-1} \text{ Hz}^{-1}$ respectively. Therefore, these regions have luminosities that are at least 3 times larger than the brightest of the super star clusters observed in local starburst galaxies (e.g., Meurer et al. 1995), and it is possible that these regions are composed of groups of star clusters. We have not corrected the observed flux densities for the effects of extinction due to dust, and the luminosities quoted should be regarded as lower limits.

However, since the extreme red color of ERO J164502+4626.4 requires a significant amount of dust, the observed morphological difference could also be produced by a spatially non-uniform dust distribution which reddens the central regions more than the outer structure. Indeed, the colors in any resolution element are redder than any reasonable stellar population, implying that the entire visible spatial extent of the galaxy is strongly reddened. It is intriguing that similar UV/optical morphological differences are observed in the inner regions of some nearby ULIRGs where they are commonly interpreted as resulting from spatial differences in the dust extinction.

3.3. Dust

The SED of ERO J164502+4626.4 is remarkably similar to those of low redshift ultraluminous galaxies like Arp 220 and Mrk 231 (figure 6), and this strongly suggests that ERO J164502+4626.4 is a dust-enshrouded system. The measured sub-millimeter flux densities at $450\mu\text{m}$, $850\mu\text{m}$ and $1350\mu\text{m}$ are greatly in excess of the power-law extrapolation of the non-thermal radio emission, and it is therefore safe to assume that the sub-millimeter flux results from thermal emission from dust heated by an AGN or in star forming regions. The mm/sub-mm spectral index is also consistent with this hypothesis.

If we assume that the SED of ERO J164502+4626.4 is indeed identical to that of the local ULIRGs, we can estimate the luminosity and mass of the warm dust responsible for the thermal emission, and attempt to constrain the star-formation rates necessary to power this galaxy. Using the template SED of an luminous *IRAS* galaxy compiled by Guiderdoni et al. (1998), we find that a least squares fit of the Guiderdoni SED to the three sub-mm points give a bolometric luminosity of $L = 7 \pm 1 \times 10^{12} h_{50}^{-2} L_{\odot}$ with reduced $\chi^2 = 1.1$ (figure 7). Almost all of this emission emerges in the far infrared: $L_{\text{FIR}} \approx 6.7 \times 10^{12} h_{50}^{-2} L_{\odot}$, where we have defined L_{FIR} as the luminosity emerging between rest wavelengths of $10\mu\text{m}$ and 2 cm. This ranks ERO J164502+4626.4 among the most luminous (unlensed) IR galaxies known, and classifies it as an ULIRG.

Note that the above estimate of the bolometric luminosity requires a large extrapolation. The sub-mm luminosity (estimated from $\nu_{rest} L_{\nu}^{rest} [850\mu\text{m}/(1+z)]$, i.e., the best-determined sub-mm flux) is $6 \times 10^{10} L_{\odot}$, and so this is an extrapolation of two orders of magnitude. However, the

sub-mm flux densities are well-fit by optically thin thermal dust emission with an emissivity law with index 1.5 (i.e., $Q_a \propto \lambda^{-1.5}$) and temperature of $T_{\text{dust}} = 40 \pm 4$ K. This dust temperature is typical of ULIRGs (Klaas & Elsasser 1993). These modified black body model fits to the sub-mm data have steeper spectra than the Guiderdoni et al. SED at $\lambda_{\text{rest}} \lesssim 40 \mu\text{m}$, and result in slightly lower values of L_{FIR} . However, although the sub-mm data are all on the Rayleigh-Jeans tail of the dust emission and therefore do not strongly constrain the dust temperature, the small χ^2 of the fit and the reasonable value of the derived dust temperature suggest that our estimate of the far-infrared luminosity is uncertain by at most a factor of two. The corresponding mass of dust is $M_{\text{dust}} \approx 7 \times 10^8 (T_{\text{dust}}/40\text{K})^{-5} h_{50}^{-2} M_{\odot}$ for optically thin emission from grains with normal interstellar parameters (Draine & Lee 1984, Hildebrand 1983).

3.4. Star Formation Rates

The star formation rates can be estimated from either the $\text{H}\alpha$ luminosity or the sub-mm continuum luminosity only if we assume that young, hot stars provide the energy source for the line and thermal continuum emission.

For our adopted cosmology ($H_0=50h_{50} \text{ km s}^{-1} \text{ Mpc}^{-1}$ and $q_0=0.5$), the luminosity in the $\text{H}\alpha$ emission line is $L_{\text{H}\alpha} \approx 4.4 \times 10^{42} h_{50}^{-2} \text{ erg s}^{-1}$. If this emission line is powered entirely by young, hot stars, then its luminosity implies a total star-formation rate of $\approx 40 h_{50}^{-2} M_{\odot} \text{ yr}^{-1}$ (Kennicutt 1983). This is almost certainly a lower limit to the true star formation rate in the galaxy, since we have not made any corrections for the dust extinction.

A more reliable estimate for the star formation rate in ERO J164502+4626.4 can be derived under the assumption that the sub-mm continuum excess is due to thermal emission from dust grains heated by young, hot stars. If stars are formed at a constant rate over $10^7 - 10^8$ yr with a Salpeter initial mass function ($\phi(m) \propto m^{-2.35}$; $0.1 \leq m \leq 100 M_{\odot}$), a luminosity of $10^{11} L_{\odot}$ corresponds to a star formation rate \dot{M} between $14 - 24 M_{\odot} \text{ yr}^{-1}$ (Leitherer and Heckman 1995). Therefore the observed bolometric luminosity corresponds to a total star formation rate of $\dot{M} = 1000 - 1800 h_{50}^{-2} M_{\odot} \text{ yr}^{-1}$ (or a factor of three smaller for the formation rate of only massive stars).

A different estimate for the formation rate of massive stars can be derived by relating the total luminosity to the mass consumption rate in early type stars. Scoville & Young (1983) derive $\dot{M}_{\text{OBA}} \approx 7.7 \times 10^{-11} (L/L_{\odot}) M_{\odot} \text{ yr}^{-1}$, which implies a formation rate of $\approx 560 (T_{\text{dust}}/40\text{K})^5 M_{\odot} \text{ yr}^{-1}$ for the massive stars. Note that this estimate does not account for the formation of lower mass stars, the mass cycled through or locked up in lower mass stars and their remnants. This star formation rate is therefore a lower limit, and as such is consistent with the estimates derived above using the Leitherer & Heckman (1983) starburst models.

If the sub-mm luminosity is indeed powered by young stars, the derived star formation rate is 26 – 45 times greater than that inferred from the $\text{H}\alpha$ luminosity; if this difference is due to dust extinction by a foreground screen, it implies an extinction of $A_V \approx 4.5$ mag. For a Galactic

extinction curve, this would imply that the intrinsic ratio of [O II] to H α of $(F_{[\text{OII}]} / F_{\text{H}\alpha})_0 \approx 1.3$, which is at the extreme limit of observed values for local star forming galaxies (e.g., Kennicutt 1992). Since the dust is more likely to be intermixed with the line-emitting gas than external to it, the extinction derived by comparing the sub-mm and H α luminosities may not be directly applicable to the reddening correction of the emission line ratios. The A_V inferred here is about 2.5 mag larger than that estimated by fitting the ERO J164502+4626.4 optical and near-IR flux densities with a reddened Sb galaxy model SED (GD96).

The star formation rate derived from the sub-mm continuum emission is extremely large and may lead us to the conclusion that the dust emission is powered by an AGN rather than by star formation. Indeed, the source of the large luminosities in local ULIRGs is still a matter of debate (e.g., Sanders & Mirabel 1996). However, there is no evidence from the existing spectroscopy that this is the case: as noted in § 3.1, the emission line ratios and widths are more typical of starburst galaxies than AGN.

The dust mass estimate from the previous section and the star formation rate derived here can be combined to yield a crude order-of-magnitude estimate for the lifetime of the starburst. Assuming that ERO J164502+4626.4 has a ‘normal’ gas-to-dust ratio of 0.01, the total mass of gas is $\sim 7 \times 10^{10} M_\odot$, and the lifetime of the burst is $t_{\text{burst}} \lesssim 1.3 \times 10^8$ yr. The total mass of stars produced is $\sim 10^{11} M_\odot$, comparable to that of a present-day massive galaxy.

In this section we have assumed that the sub-mm continuum emission is due to thermal emission from dust heated by young, hot stars. One curious property of ERO J164502+4626.4 which may be relevant to this hypothesis is that the rest frame 60 μm emission predicted by the dust emission and the nonthermal radio emission at a rest wavelength of 6 cm (extrapolated from the flux density observed at 1.4 GHz assuming a $S_\nu \propto \nu^{-0.7}$ synchrotron spectrum) does not follow the well-known 60 μm – 6 cm correlation obeyed by local star forming galaxies (e.g., de Jong et al. 1985). The rest frame 6 cm emission predicted by this correlation for ERO J164502+4626.4 is $\approx 300 \mu\text{Jy}$, more than an order of magnitude above the detected radio emission (Table 2). The only ways of decreasing the predicted 60 μm emission would be to decrease the dust temperature and increase the dust optical depth, both of which result in worse fits to the sub-mm data. The existing *ISO* data may be able to help constrain the dust temperature and optical depth estimates (Ivison et al. 1999). This issue can also be resolved with better far-infrared observations of ERO J164502+4626.4, which will soon be possible with the *Space Infrared Facility (SIRTF)*.

If the large deviation from the 60 μm – 6 cm correlation is real, its interpretation is unclear. It is unlikely that this deviation is due to the sub-mm flux being heated by an AGN instead of a starburst, since in the local universe AGN tend to depart from the correlation by having excess nonthermal radio emission, not excess far-infrared emission (e.g., Dey & van Breugel 1994). Some local ULIRGs (e.g., Arp 220) do show low frequency turnovers in their radio spectra which are generally attributed to thermal absorption of the radio emission (Sopp & Alexander 1991). On the other hand, the first reliably identified sub-mm selected high redshift galaxy, SMM J02399–0136

($z = 2.80$; Ivison et al. 1998b), has a ‘normal’ $60\mu\text{m} - 6\text{ cm}$ ratio, yet shows some evidence for an AGN contribution to the total emission. Since the far-infrared flux densities are poorly constrained at present, and the origin of the correlation in local galaxies is also not completely understood, we hesitate to draw any firm conclusions from this observation.

3.5. Cosmological Implications

Measurements of the global star-formation history of the Universe, using deep redshift surveys, e.g., the Canada France Redshift Survey (Lilly et al. 1996) reaching $z \simeq 1$, the statistics of Lyman-limit galaxies (Steidel & Hamilton 1992) at $z = 3.4$, the Hubble Deep Field (HDF) $2.5 < z < 4$ (Madau et al. 1996, Connolly et al. 1997), imply that the star-formation and metal-production rates were about 10 times greater at $z \simeq 1$ than in the local Universe, that they reach a maximum somewhere in the redshift range $1 \lesssim z \lesssim 1.5$ and remain roughly constant (or perhaps slowly decline) at higher redshifts (Steidel et al. 1999).

These conclusions, which are based almost entirely on samples selected at optical and near-UV wavelengths, may be misleading (Smail, Ivison & Blain 1997; Blain et al. 1999a). Absorption by dust in regions of star-formation may have distorted our picture of galaxy evolution in the high- and low-redshift Universe in two ways. First, neglect of dust leads to an underestimate of the the star-formation rate in known high- and low-redshift objects. Second, it is possible that an entire population of heavily dust-enshrouded high-redshift objects, such as EROs, has escaped undetected in the optical/UV surveys.

A useful diagnostic of the redness of the SED is the rest frame infrared-to-blue luminosity ratio (L_{FIR}/L_B), where $L_{FIR} \equiv \nu L_\nu$ at $\lambda_{\text{rest}} = 80\mu\text{m}$ and $L_B \equiv \nu L_\nu$ at $\lambda_{\text{rest}} = 4400\text{\AA}$. By this measure, the reddest galaxy in the UGC is Arp 220 ($L_{FIR}/L_B \approx 60$; Soifer et al. 1984). The mean L_{FIR}/L_B value for the ultraluminous sample is 25 (Sanders et al. 1987), and the reddest ultraluminous galaxy in the *IRAS Bright Galaxy Catalog* is IRAS 12112+0305, which has $L_{FIR}/L_B \approx 70$. If we estimate L_B for ERO J164502+4626.4 by interpolating the observed *I* and *J* fluxes, we find that ERO J164502+4626.4 has $f_B \approx 2.3 \mu\text{Jy}$. Hence, $L_B \approx \nu L_\nu(4400\text{\AA}) \approx 2.2 \times 10^{10} L_\odot$, and $L_{FIR}/L_B \approx 300$! The name ERO is therefore justified for this remarkable object.

The relevance of ERO J164502+4626.4 to cosmology and galaxy formation depends critically on the space density of the ERO population, which is highly uncertain at present. Under the assumptions that the EROs form a homogeneous population and the redshift and sub-mm luminosity of ERO J164502+4626.4 is typical of this class, GD96 estimated that the space density of these objects is $\rho_{\text{ERO}} \approx 2.1 \times 10^{-4} h_{50}^3 \text{ Mpc}^{-3} \text{ mag}^{-1}$. Hence, EROs may be more abundant than the *IRAS* ultraluminous galaxies and quasars by two orders of magnitude. If the star formation rate for these galaxies is similar to that observed in ERO J164502+4626.4 (i.e., $\dot{M} > 580 M_\odot \text{ yr}^{-1}$), the star formation rate at $z = 1.4$ associated with the ERO population is $\gtrsim 0.1 h_{50} M_\odot \text{ yr}^{-1} \text{ Mpc}^{-3}$. This sub-mm estimate of the star formation density exceeds the rest-frame UV estimates of the

high-redshift star formation rate (from the CFRS and HDF surveys) by more than a factor of six. It is noteworthy that this crude estimate is roughly consistent with the predictions of Pei & Fall (1995) (see also Hughes et al. 1998).

Deep surveys at $850\mu\text{m}$ of the sub-mm sky have resulted in the detection of several faint sources ($\gtrsim 4$ mJy), about 20% of which appear to have no obvious optical counterpart brighter than $I \sim 25$ (Smail et al. 1998). It is possible that these ‘missing’ optical identifications are galaxies similar to ERO J164502+4626.4, perhaps even fainter at optical wavelengths, but with similarly strong thermal dust emission at sub-mm wavelengths. Since the cumulative surface density of the sub-mm continuum emitters with $850\mu\text{m}$ flux densities ≥ 4 mJy is $2.4 \pm 1.0 \times 10^3 \text{ deg}^{-2}$, the surface density of the optically faint fraction is $\sim 480 \text{ deg}^{-2}$ (estimates here are based on the surface density determined by Blain et al. 1999b; however, see Barger et al. 1998 for a lower estimate). The surface density of EROs is highly uncertain: Hu & Ridgway (1994) estimated that the surface density of objects with $I - K \geq 6$ and $K \leq 19$ is $\approx 36 \text{ deg}^{-2}$, whereas estimates of the surface density of less extreme EROs (with $R - K \geq 6$) discovered serendipitously tend to be larger by at least an order of magnitude (e.g., Dey, Spinrad & Dickinson 1995; Knopp & Chambers 1997; Beckwith et al. 1998). The roughly comparable space densities of these two populations suggests that it is possible that EROs comprise a significant fraction, perhaps all, of the optically faint sub-mm emitters discovered in recent surveys. A large fraction of both local ULIRGs and distant SCUBA sources (Smail et al. 1998) appear to be interacting or merging systems, perhaps similar to ERO J164502+4626.4.

Since the sub-mm sources thus far detected at flux densities $\gtrsim 0.5$ mJy arguably account for upto 100% of the $850\mu\text{m}$ cosmic sub-mm background (Smail et al. 1997, Blain et al. 1999), the ERO population may comprise a substantial component of the resolved emission. The relevance of the properties of ERO J164502+4626.4 for our general understanding of both the ERO and sub-mm populations will hinge on whether it represents a particularly high luminosity or low redshift member of this group.

The very red SED of ERO J164502+4626.4 also implies that it will be extremely difficult to detect the most actively star-forming galaxies at higher redshifts, since they may be completely enshrouded by dust and undetectable at optical and near-IR wavelengths. For instance, if ERO J164502+4626.4 were at $z = 5$, it would have a $K \approx 25.8$ and $I > 32$ ($H_0=50$, $q_0=0.5$), and therefore undetectable in even the deepest existing ground- and space-based surveys. In contrast, the large negative sub-mm k-correction would imply that the $850\mu\text{m}$ flux density of such an object would be ~ 3 mJy, comparable to that at $z = 1.44$. The existence of dusty star-forming systems at $z \gtrsim 5$ is not an unrealistic expectation: the $z = 5.34$ galaxy 0140+326RD1 (Dey et al. 1998) has been recently argued to be a dusty star-forming system based on its red $I - J$ color (Armus et al. 1998). It is important to note, however, that the inferred dust content of 0140+326RD1 is much lower than that of ERO J164502+4626.4: the implied extinction is $A_V \approx 0.5$ mag for 0140+326RD1, compared with $A_V \approx 4.5$ for ERO J164502+4626.4. Investigating the properties of the higher redshift counterparts of systems like ERO J164502+4626.4 will require sensitive ground-based sub-mm facilities with high-angular resolution and space-based telescopes operating at near-IR and mid-IR

wavelengths. In the near-future, the *Space Infrared Telescope Facility (SIRTF)* will provide flux density observations of EROs at mid- and far-infrared wavelengths ($\sim 3 - 180 \mu\text{m}$) allowing us to place more critical constraints on the dust masses, temperatures and source luminosities, and perhaps determine the relationship of these objects to present-day galaxies.

4. Conclusion

We have presented new optical, near-IR and sub-mm observations of ERO J164502+4626.4 (object # 10 in Hu & Ridgway 1994), an extremely red object in the field of the QSO PC 1643+4631A. The new optical and near-IR spectroscopy show that ERO J164502+4626.4 is a distant galaxy lying at a redshift of $z = 1.44$. The peculiar rest frame near-UV and far-red morphologies suggest that ERO J164502+4626.4 is a disturbed or interacting system. The far-IR and sub-mm evidence are consistent with the hypothesis that this ERO is a dust-enshrouded object, with its luminosity ($L \approx 7 \times 10^{12} h_{50}^{-2} L_{\odot}$) powered by either a starburst or an AGN. The existing spectral data for ERO J164502+4626.4 show no strong evidence for AGN emission at rest-frame near-UV or optical wavelengths. If the observed sub-mm continuum flux is due to optically thin thermal emission from dust heated by a young, star forming population, the inferred star formation rate is extremely large ($1000 - 2000 M_{\odot} \text{yr}^{-1}$). In all its known properties, ERO J164502+4626.4 appears to be a high-redshift luminous counterpart of the dusty, ultraluminous galaxies discovered in the local Universe by *IRAS*. Although it is difficult to draw general conclusions from a single object, less luminous or higher redshift galaxies similar to ERO J164502+4626.4 may be missed from even the deepest existing optical and surveys. It is important to determine the space densities of these EROs and their relevance to our understanding of galaxy formation and evolution in the distant universe.

We thank Brett Huggard, Gillian Rosenthal & Dick Joyce for their expert assistance during our KPNO observing runs, Richard Elston for advice on using CRSP, the numerous people who have made possible the process of obtaining and calibrating *HST* WFPC2 data, and the JCMT staff for assistance during the SCUBA observations. We are grateful to Wayne Wack, David Sprayberry and Bob Goodrich for their help with the Keck LRIS observations. We thank Bill Reach for help with determining the Galactic far-infrared foreground towards ERO J164502+4626.4, and the referee, Peter Eisenhardt, for constructive comments on our manuscript. AD acknowledges the support of NASA HF-01089.01-97A and partial support from a Postdoctoral Research Fellowship at NOAO, operated by AURA, Inc. under cooperative agreement with the NSF. JRG acknowledges support from NASA GO-06598.02-95A. The W. M. Keck Observatory is a scientific partnership among the University of California, the California Institute of Technology, and the National Aeronautics & Space Administration, and was made possible by the generous financial support of the W. M. Keck Foundation. The James Clerk Maxwell Telescope is operated by The Joint Astronomy Centre on behalf of the Particle Physics and Astronomy Research Council of the United Kingdom, the Netherlands Organisation for Scientific Research and the National Research Council of Canada.

REFERENCES

- Aragon-Salamanca, A., Ellis, R. S., Schwartzenberg, J.-M., & Bergeron, J. A. 1994, *ApJ*, 421, 27
- Armus, L., Matthews, K., Neugebauer, G. & Soifer, B. T. 1998, *ApJ*, 506, L89
- Barger, A. J. et al. 1998, *Nature*, 394, 248
- Barvainis, R., Antonucci, R., Hurt, T., Coleman, P., & Reuter, H.-P. 1995, *ApJ*, 451, L9
- Beckwith, S. V. W., Thompson, D., Manucci, F. & Djorgovski, S. G. 1998, *ApJ*, 504, 107
- Blain, A. W., Kneib, J.-P., Ivison, R. J., & Smail, I. 1999a, *ApJ*, in press (astro-ph/9812412)
- Blain, A. W., Smail, I., Ivison, R. J. & Kneib, J.-P. 1999b, *MNRAS*, 302, 632
- Broadhurst, T., & Lehar, J. 1996, *ApJ*, 450, L41
- Cimatti, A., Andreani, P., Röttgering, H. & Tilanus, R. 1998, *Nature*, 392, 895
- Connolly, A.J., Szalay, A.S., Dickinson, M. SubbaRao, M.V, Brunner, R.J. 1997, *ApJ*, 486, L11
- Cowie, L. L., Gardner, J. P., Hu, E. M., Songalia, A., Hodapp, K.-W., & Wainscoat, R. J. 1994, *ApJ*, 434, 114
- Dey, A., Spinrad, H., & Dickinson, M. 1995, *ApJ*, 440, 515
- Dey, A., Spinrad, H., Graham, J. R. & Chaffee, F. H. 1998, *ApJ*, 498, L93
- Dey, A. & van Breugel, W. 1994, in “Mass Transfer Induced Activity in Galaxies”, I. Shlosman, ed. (Cambridge Univ Press) p.263
- Draine, B. T. & Lee, H. M. 1984, *ApJ*, 285, 89
- Eisenhardt, P. R. M., & Dickinson, M. 1992, *ApJ*, 399, L47
- Eisenhardt, P., Elston, R., Stanford, S. A., Dickinson, M., Spinrad, H., Stern, D., & Dey, A. 1998, in “The Birth of Galaxies,” Proceedings of the Xth Recontres de Blois, eds. B. Guiderdoni, F. R. Bouchet & T. X. Thuan, Paris: Editions Frontieres, in press.
- Elston, R., Rieke, G. H., & Rieke, M. J. 1988, *ApJ*, 331, L77
- Elston, R., Rieke, M. J., & Rieke, G. H. 1989, *ApJ*, 341, 80
- Elston, R., Rieke, G. H., & Rieke, M. J. 1991, in *Astrophysics with Infrared Arrays*, ed. R. Elston (ASP Conf. Ser., 14), 3
- Fixsen, D. J., Dwek, E., Mather, J. C., Bennett, C. L. & Shafer, R. A. 1998, *ApJ*, in press (astro-ph/9803021)
- Frayser, D. T. 1996, PhD Thesis, University of Virginia
- Graham, J. R., et al. 1994, *ApJ*, 420, L5
- Graham, J. R., & Dey, A. 1996, *ApJ*, 471, 720
- Graham, J. R. & Liu, M. C. 1995, *ApJ*, 449, L29
- Guiderdoni, B., Hivon, E., Bouchet, F. R., Maffei, B. 1998, *MNRAS*, 295, 877

- Hauser, M. G. et al. 1998, ApJ, in press (astro-ph/9806167)
- Hildebrand, R. H. 1983, QJRAS, 24, 267
- Holland, W. S. et al. 1998, MNRAS, submitted
- Holtzman, J. et al. , 1995, PASP, 107, 156
- Hu, E. M., & Ridgway, S. E. 1994, AJ, 107, 1303
- Hughes, D. et al. 1998, Nature, 394, 241
- Iverson, R. J. 1995, MNRAS, 275, L33
- Iverson, R. J. et al. 1998a, ApJ, 494, 211
- Iverson, R. J. et al. 1998b, MNRAS, 298, 583
- Iverson, R. J. et al. 1999, in preparation
- Joyce, R. 1995, “Cryogenic Spectrometer User Manual”, NOAO
- Kennicutt, R. C. 1983, ApJ, 272, 54
- Kennicutt, R. C. 1992, ApJS, 79, 255
- Kessler, M. F., et al. 1996, A&A, 315, L27
- Klaas, U. & Elsasser, H. 1993, AA, 280, 76
- Knopp, G. P. & Chambers, K. C. 1997, ApJS, 109, 367
- Lancon, A. & Rocca-Volmerange, B. 1992, A&AS, 96, 593
- Lemke, D., et al. 1996, A&A, 315, L64
- Leitherer, C. & Heckman, T. M. 1996, ApJS, 96, 9
- Lilly, S.J., Le Fèvre, O., Hammer, F., Crampton, D. 1996, ApJ, 460, L1
- Liu, C. T. & Kennicutt, R. C. 1995, ApJ, 450, 547
- Madau, P. et al. 1996, MNRAS, 283, 1388
- Massey, P., Strobel, K., Barnes, J. V. & Anderson, E. 1988, ApJ, 328, 315
- Massey, P. & Gronwall, C. 1990, ApJ, 358, 344
- McCarthy, P. J., Persson, S. E., & West, S. C. 1992, ApJ, 386, 52
- Meurer, G. R., Heckman, T. M., Leitherer, C., Kinney, A., Robert, C. & Garnett, D. R. 1995, AJ, 110, 2665
- Oke, J. B., et al. 1995, PASP, 107, 375
- Pei, Y. C. & Fall, S. M. 1995, ApJ, 454, 69
- Puget, J. L. et al. 1996, A&A, 308, L5
- Rowan-Robinson M., et al. 1993, MNRAS, 261, 513
- Sanders & Mirabel 1996, ARAA, 34, 749

- Schlegel, D. J., Finkbeiner, D. P., & Davis, M. 1998, *ApJ*, 500, 525
- Smail, I., Ivison, R. J. & Blain, A. W. 1997, *ApJ*, 490, L5
- Smail, I., Ivison, R. J., Blain, A. W. & Kneib, J.-P. 1998, *ApJ*, 507, L21
- Sopp, H. M. & Alexander, P. 1991, *MNRAS*, 251, 112
- Soifer, B. T., et al. 1984, *ApJ*, 283, L1
- Soifer, B. T., et al. 1992, *ApJ*, 399, L55
- Steidel, C.C., Hamilton, D. 1992, *AJ*, 104, 941
- Steidel, C. C., Adelberger, K. L., Giavalisco, M., Dickinson, M. & Pettini, M. 1999, *ApJ* in press
(astro-ph/9811399)
- Trauger, J. T. et al. , 1994, *ApJ*, 435, L3
- Yamada, T., Tanaka, I., Aragon-Salamanca, A., Kodama, T., Ohta, K., & Arimoto, N. 1997, *ApJ*,
487, L125

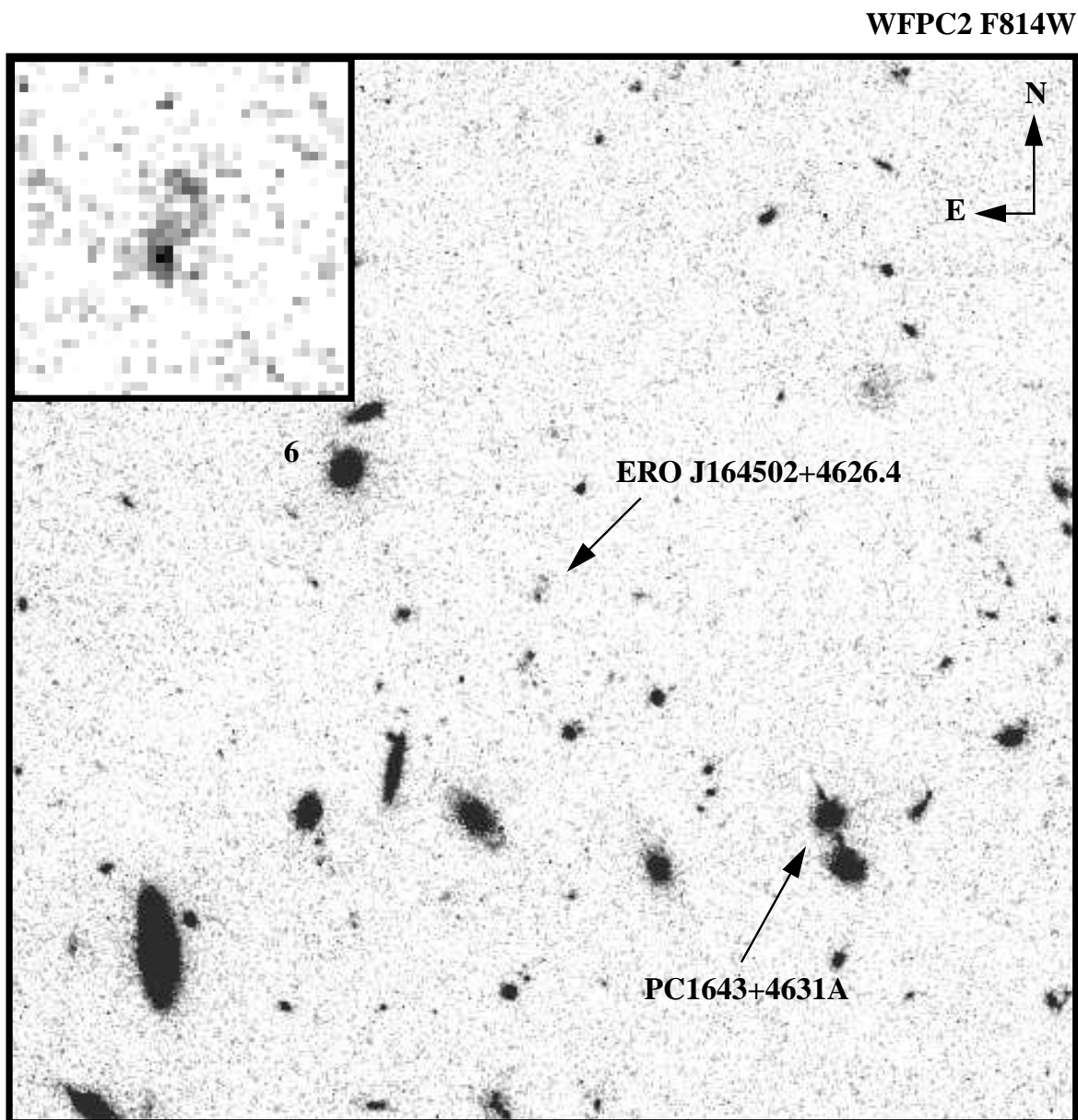


Fig. 1.— *HST* WFPC2 image of ERO J164502+4626.4 (object 10 in Hu & Ridgway 1994) obtained through the F814W filter. The field of view shown is 50'' on a side, and the ERO and the QSO PC1643+4631A are labelled. North is up and east is to the left. ERO J164502+4626.4 (“HR 10”) is located at $\alpha = 16^h 45^m 02^s 36$, $\delta = +46^\circ 26' 25''.5$ (J2000), and the offset from the QSO is $\Delta\alpha = +13''.85$, $\Delta\delta = +10''.27$. The galaxy labelled “6” was used for aligning the dithered IR spectra (see text). The inset, 4'' on a side, shows ERO J164502+4626.4.

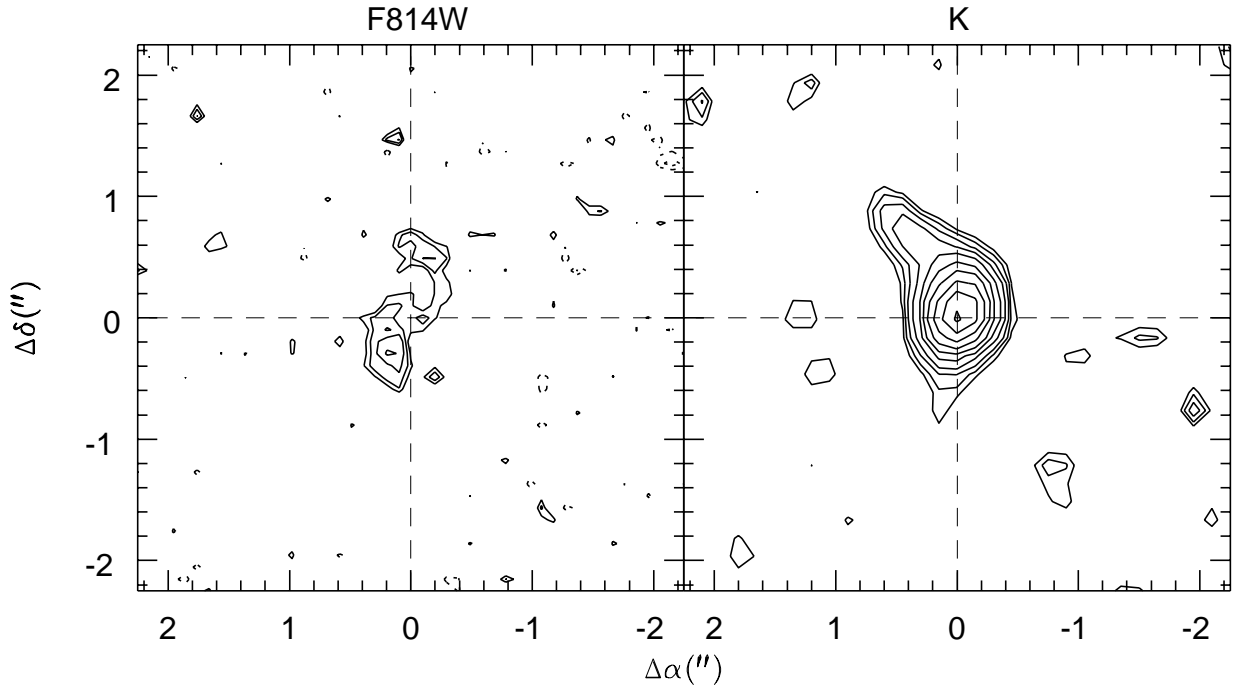


Fig. 2.— This figure presents a comparison of the observed K and F814W morphologies of ERO J164502+4626.4. The left panel shows a contour plot of the HST WFPC2 image obtained through the F814W filter. The contour levels are drawn at levels $(2,3,4,5,6,7,8,9,10) \times \sigma_{sky}$, where $\sigma_{sky} = 25.56 AB \text{ mag arcsec}^{-2}$. Negative contours are represented by dotted lines. The right panel shows a contour plot of the Lucy-deconvolved K -band image from Graham & Dey (1996). The contour levels are drawn as in the left panel, but with σ_{sky} equivalent to $21.38 \text{ mag arcsec}^{-2}$. The resolution of the F814W image is $\approx 0''.1$ whereas the resolution of the Lucy-deconvolved K -band image is $\approx 0''.28$. Note that the morphologies are different and that the peak of the K -band emission occurs in a region of low optical emission.

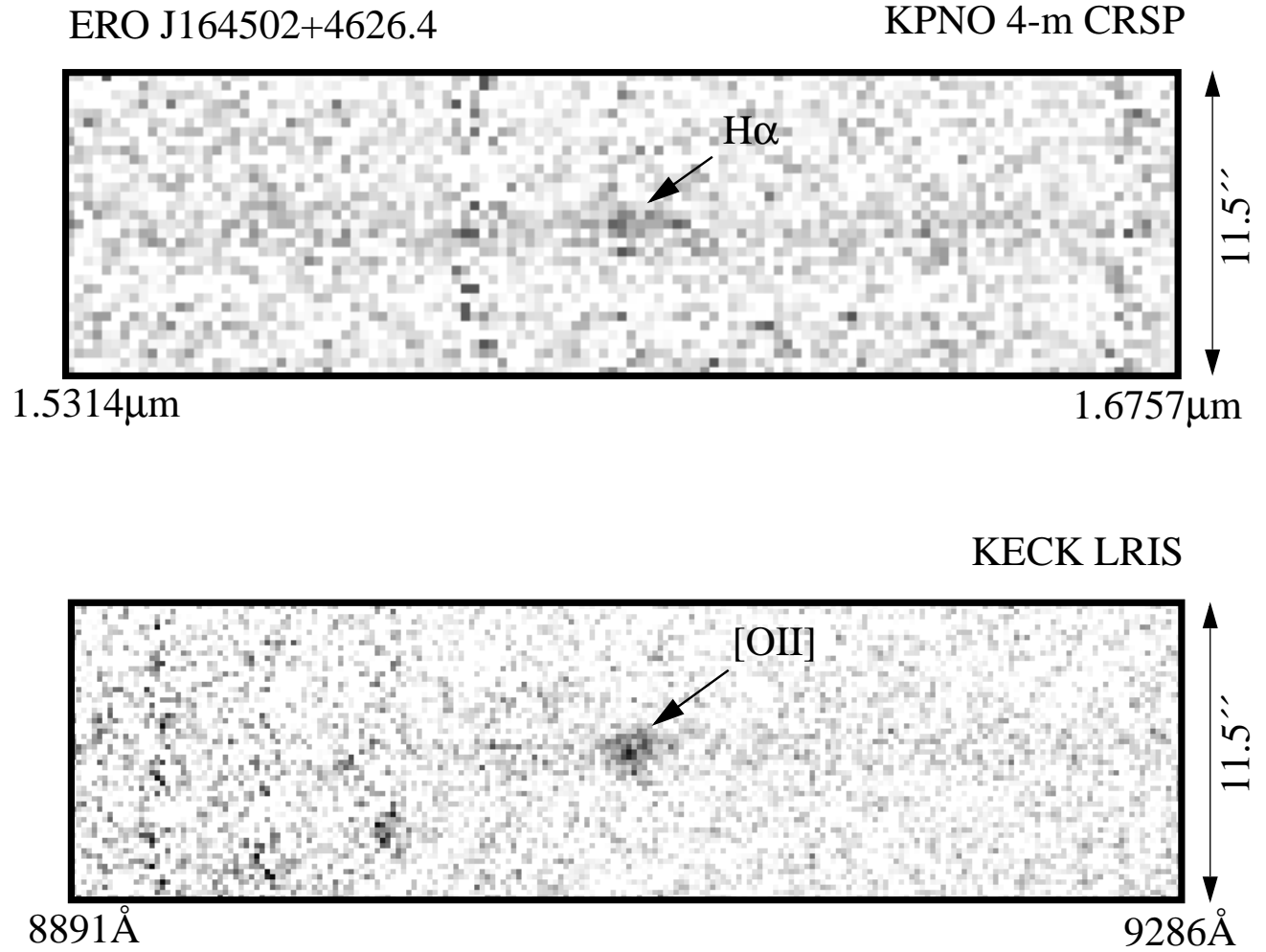


Fig. 3.— The above panels present portions of the two-dimensional spectra of ERO J164502+4626.4 showing the emission line detections. The upper panel shows the detection of the H α emission line in the coadded near-IR spectrum obtained using CRSP on the KPNO 4-m telescope. The lower panel shows the detection of the [OII] $\lambda\lambda$ 3726,3729 emission doublet in the optical spectrum obtained using LRIS on the Keck II Telescope.

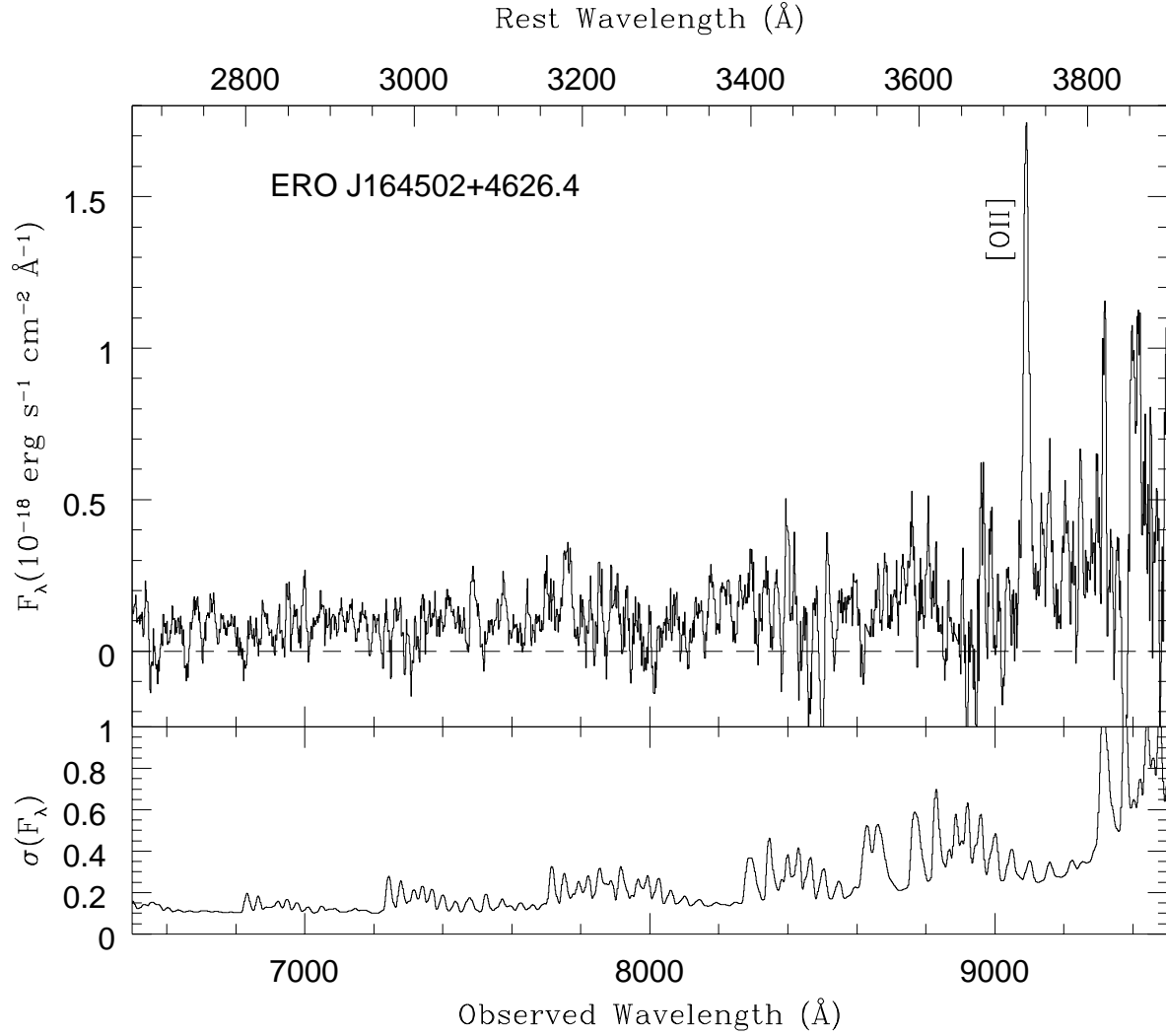


Fig. 4.— Optical spectrum of ERO J164502+4626.4 obtained using LRIS on the Keck II Telescope. The upper panel shows the observed spectrum extracted in a $1''.0 \times 1''.7$ aperture smoothed using a 13\AA width boxcar filter, and the bottom panel shows the corresponding 1σ error spectrum. The [OII] $\lambda\lambda 3726, 3729$ emission doublet is marked.

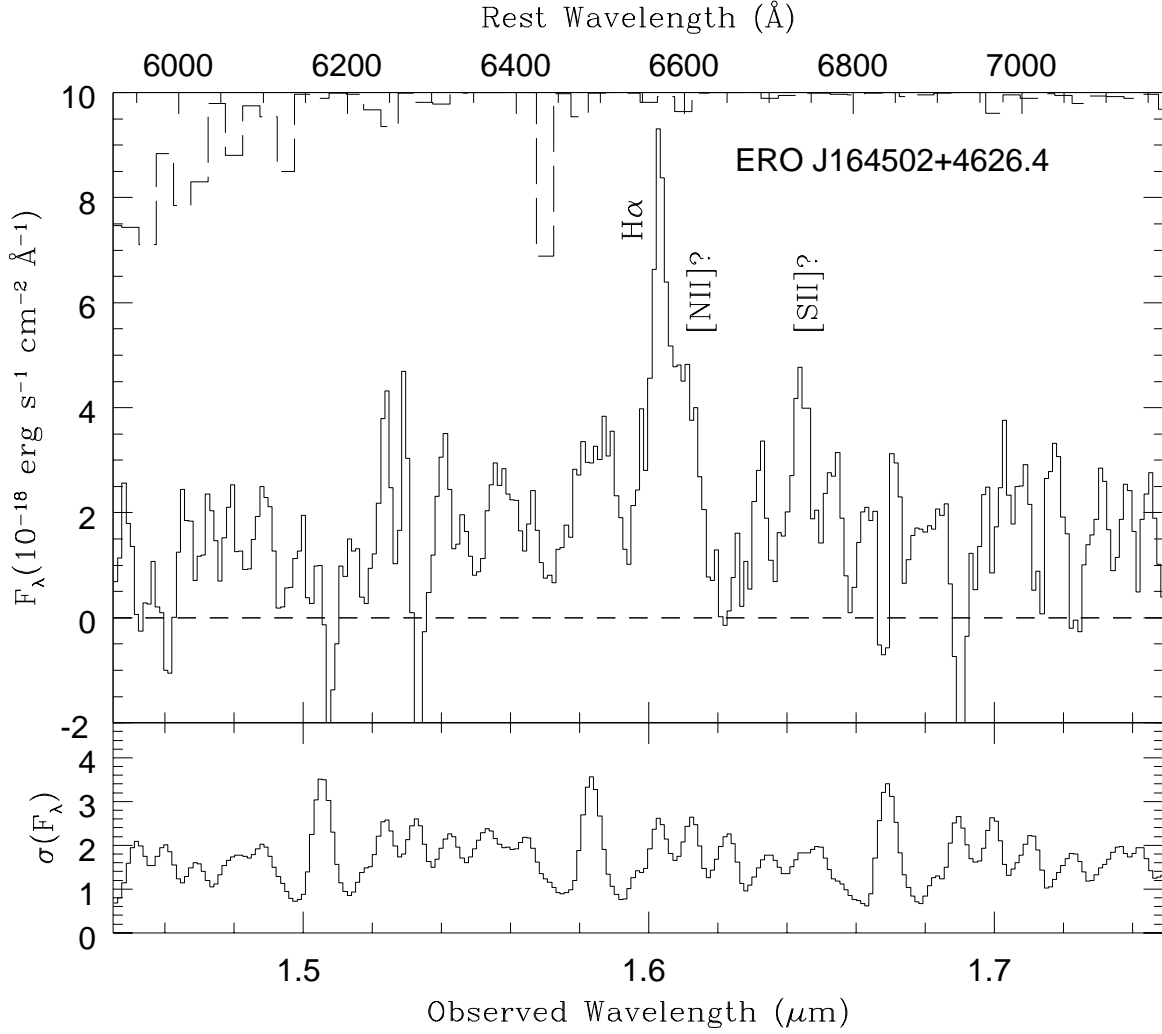


Fig. 5.— Near-IR spectrum of ERO J164502+4626.4 obtained using CRSP on the KPNO 4-m telescope. The upper panel shows the observed spectrum extracted in a $1''.0 \times 1''.7$ aperture and smoothed using a 36\AA width boxcar filter (solid line), along with the relative atmospheric transmission (long dashed line). The bottom panel shows the corresponding 1σ error spectrum which is dominated by the OH telluric emission lines. The $\text{H}\alpha$ emission line and locations of the [NII] λ 6584 and [SII] $\lambda\lambda$ 6717,6731 emission doublet are marked.

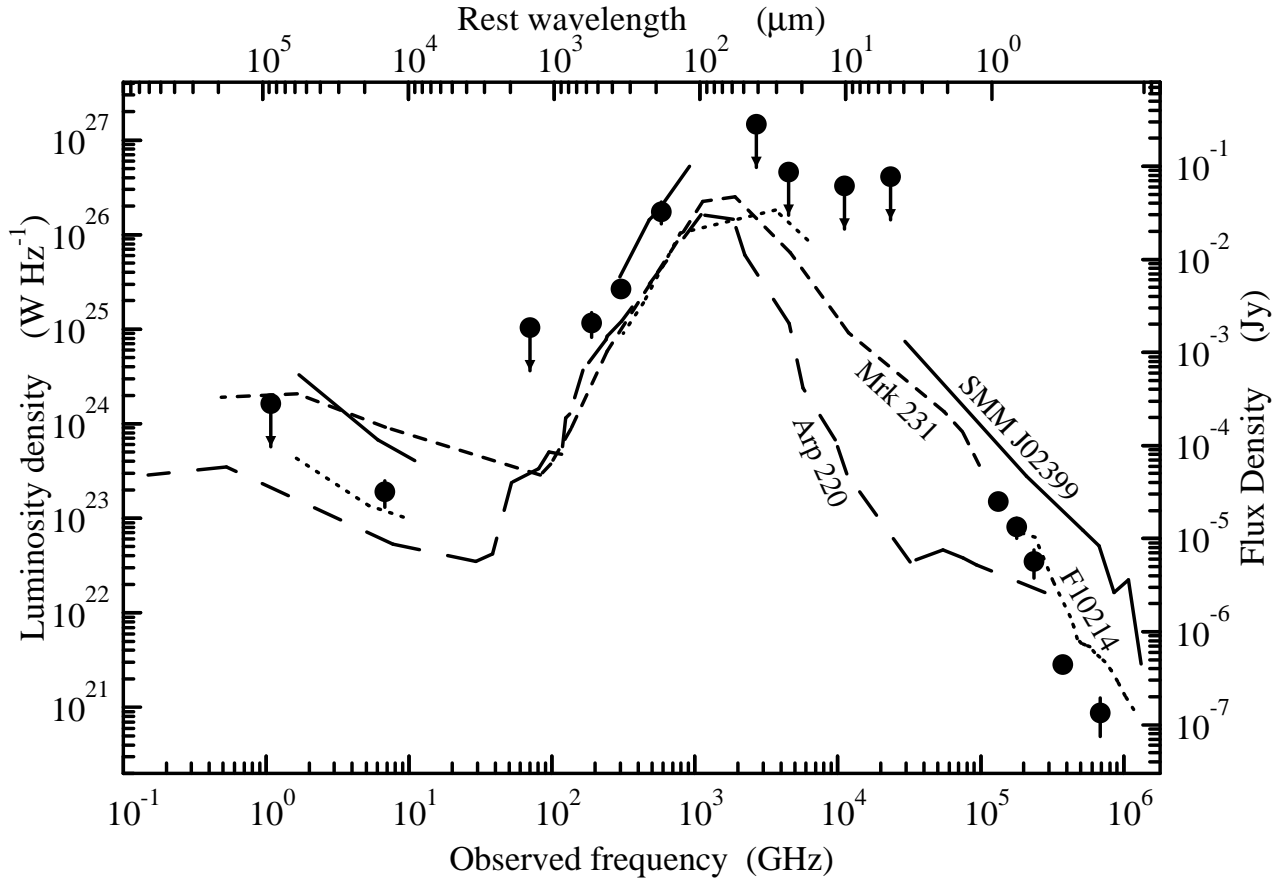


Fig. 6.— The SED of ERO J164502+4626.4 between the radio and optical wavebands, represented by filled circles. The right-hand scale gives flux densities for ERO J164502+4626.4. For comparison, we have plotted the SEDs of the ultraluminous *IRAS* sources F 10214+4724 (Rowan-Robinson et al. 1993; Barvainis et al. 1995), Mrk 231 and Arp 220 (D. H. Hughes priv. comm.), and SMM 02399–0136 (Ivison et al. 1998b) with units of luminosity density (*left-hand scale*). These lines are broken in regions where only upper limits are available. For F 10214+4724 and SMM 02399–0136 the SEDs are corrected for lensing by factors of 30 and 2.5 respectively (e.g., Graham & Liu 1995; Broadhurst & Lehar 1996; Ivison et al. 1998b).

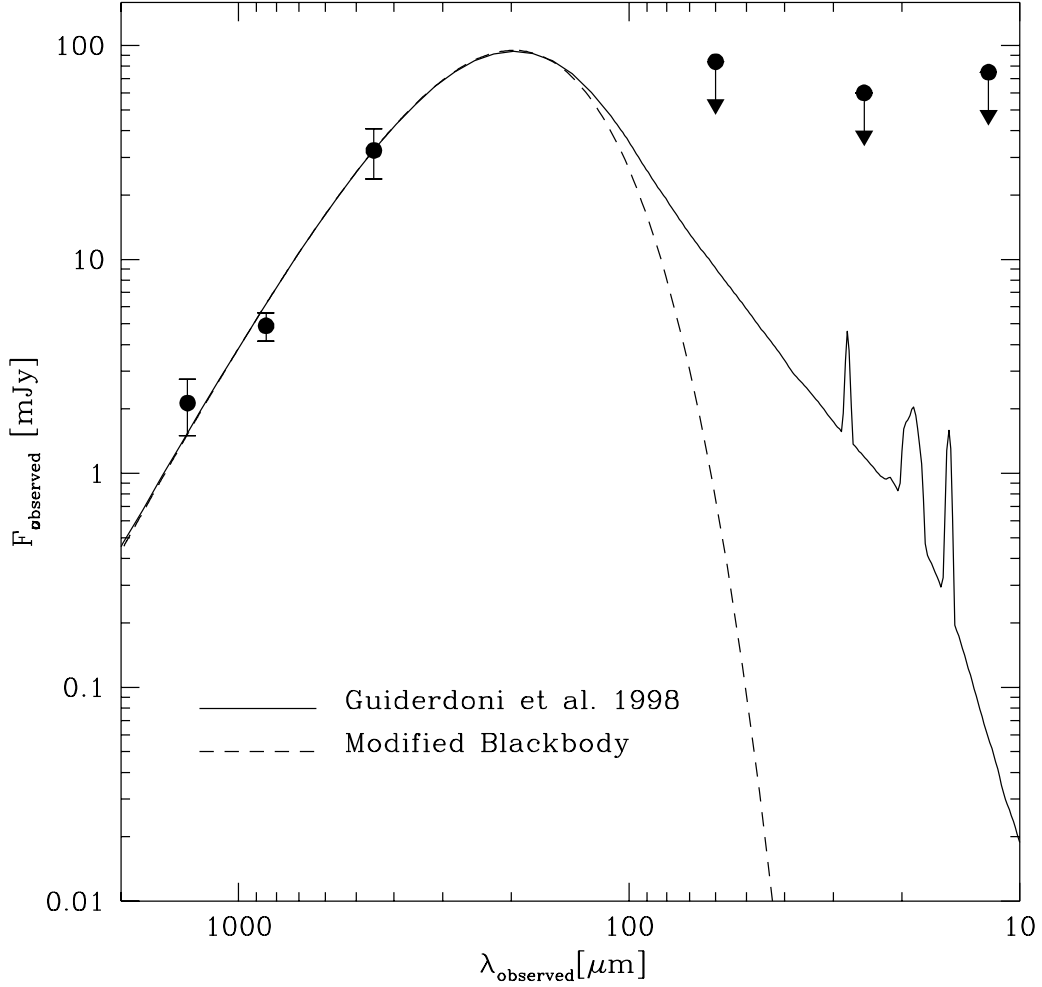


Fig. 7.— The rest frame far-infrared SED of ERO J164502+4626.4 wavebands (filled circles) compared with a Guiderdoni et al. (1998) semi-empirical SED for IR luminous galaxies and a modified blackbody ($F_\nu \propto B_\nu[1 - \exp\{-(\nu/\nu_0)^\beta\}]$) of temperature $T = 40$ K and emissivity index $\beta = 1.5$. The models shown were fitted to the three sub-mm flux density measurements.

Table 1. Emission Line Measurements of ERO J164502+4626.4¹

Line	λ_{obs} Å	Redshift	Flux $10^{-17} \text{erg s}^{-1} \text{cm}^{-2}$	FWHM km s^{-1}	$W_{\lambda, \text{rest}}$ ² Å
[OII] $\lambda\lambda$ 3726,3729	9090.6 \pm 0.9	1.439	2.6 \pm 0.4	420 \pm 100	47 \pm 5
H α	16030 \pm 7	1.443	33 \pm 8	597 \pm 140	89 \pm 20
[NII] λ 6584	16081.1 ³		14 \pm 5	597 ³	37 \pm 13
[SII] $\lambda\lambda$ 6717,6731	16437 \pm 7	1.444	14 \pm 6	532 \pm 250	38 \pm 17

¹All quoted measurements are based on Gaussian fits to the emission lines. The spectra were obtained through 1.''0 wide slits, and the spectral extractions used in these measurements are 1.''7 wide in P.A.=66.2 ([OII]) and P.A.=59.3 (H α , [NII] and [SII]).

²Rest-frame equivalent widths assume $z = 1.440$.

³The central wavelength and width of the [NII] λ 6584 emission line are fixed with respect to the derived values for the H α emission line.

Table 2. Photometry of ERO J164502+4626.4

Observed Wavelength	Rest Wavelength	Flux Density	Detector/Instrument	Reference
4400Å	1800Å	0.16 \pm 0.07 μ Jy		GD96, Hu & Ridgway (1992)
7930Å	3250Å	0.52 \pm 0.06 μ Jy	WFPC2/ <i>HST</i>	This paper
1.2 μ m	4920Å	6.4 \pm 2.1 μ Jy		GD96, Hu & Ridgway (1992)
1.6 μ m	6560Å	14.8 \pm 3.6 μ Jy		GD96, Hu & Ridgway (1992)
2.2 μ m	9010Å	27.7 \pm 0.6 μ Jy		GD96
12 μ m	4.9 μ m	< 75 mJy	<i>IRAS</i>	
25 μ m	10.2 μ m	< 60 mJy	<i>IRAS</i>	
60 μ m	24.6 μ m	< 84 mJy	<i>IRAS</i>	
100 μ m	41.0 μ m	< 270 mJy	<i>IRAS</i>	
450 μ m	184 μ m	32.3 \pm 8.5 mJy	SCUBA/JCMT	This paper
850 μ m	348 μ m	4.89 \pm 0.74 mJy	SCUBA/JCMT	This paper
1350 μ m	553 μ m	2.13 \pm 0.63 mJy	SCUBA/JCMT	This paper
3.6 cm	1.5 cm	35 \pm 11 μ Jy		Frayser (1996)
20 cm	8.6 cm	< 300 μ Jy		Frayser (1996)